Chinese Chemical Letters 31 (2020) 953–960

Contents lists available at ScienceDirect

Chinese Chemical Letters

journal homepage: www.elsevier.com/locate/cclet

Review

Recent advances of MXene as promising catalysts for electrochemical nitrogen reduction reaction

Jie Sun[1], Wenhan Kong[1], Zhaoyong Jin, Yaqian Han, Liangyu Ma, Xiaoteng Ding, Yusheng Niu, Yuanhong Xu*

College of Materials Science and Engineering, College of Life Sciences, Qingdao University, Qingdao 266071, China

ARTICLE INFO

Article history:
Received 6 November 2019
Received in revised form 22 December 2019
Accepted 6 January 2020
Available online 17 January 2020

Keywords:
Nitrogen reduction reaction
Electrocatalysis
MXene
Nanomaterials
Two-dimensional nanomaterials

ABSTRACT

Electrochemical reduction of N_2, as an eco-friendly alternative, not only allows the use of protons in water as a source of hydrogen under mild conditions but also can be driven by renewable electric energy. The major challenge is to identify high-efficiency electrocatalysts. MXene is a new class of 2D transition metal carbides, nitrides, and carbonitrides that have received significant attention in electrocatalysis. The investigations on MXene in electrocatalytic nitrogen fixation are rapidly proceeding, and some breakthroughs have emerged very recently due to MXenes' satisfactory catalytic activity. Here, the recent progress concerning the MXene-based catalysts for electrochemical N_2 reduction reaction (NRR) is highlighted. In regards to giving guidelines for exploring more efficient MXene-based catalysts for the NRR, the fabrication and surface modification of MXene are discussed. Besides, the shortcomings and challenges of current research are summarized and the future research directions are prospected.

1. Introduction

The escalating consumption of fossil fuels has driven the development of methods for energy production that aim at enhancing sustainability and reducing negative impacts on the environment [1,2]. NH_3 synthesis is a highly crucial process to chemical production and agriculture. Meanwhile NH_3 supplies a green energy carrier and potential transportation fuel [3–6]. Thus far, the conventional Haber–Bosch process remains the only industrial process for large-scale NH_3 production. This process was conducted under extreme reaction conditions (350–550 °C and 150–350 atm) and used high-purity N_2 and H_2 as the feed [5,7], consuming 1%–2% of the worldwide annual energy and contributing to more than 1% of global greenhouse gas emission [8]. It is thus urgently required to develop environment-friendly and less energy-demanding methodologies for NH_3 synthesis. As an eco-friendly alternative, electrochemical N_2 reduction that uses protons in water as the hydrogen source under mild conditions not only allows for the possibility of artificial N_2 fixation, but also can be powered by renewable electric energy. Nevertheless, the development of electrochemical nitrogen reduction reaction (NRR) is significantly restricted by the intrinsic chemical inertness of N_2 molecules [9–11]. Considerable attention has been paid to identify electrocatalysts for NRR with high activity, stability, and excellent selectivity [12,13].

Two-dimensional (2D) materials have attracted broad scientific interest in the past decade for their excellent physical, electronic and chemical properties [14–17]. They have emerged as an interesting candidate in the electrochemical NRR, such as molybdenum disulfide, graphene, and metal-organic frameworks (MOFs) [18–20]. It is worth noting that a new member joined the 2D material family in 2011, namely 2D transition metal carbides, nitrides, and carbonitrides, known as MXene, and has developed very rapidly in the last eight years [21–23]. MXenes were expected to be promising candidates for electrocatalytic NRR applications due to their exceptional properties, including large surface area, rich composition and surface chemistry, adjustable structure, and excellent stability [24–26]. The investigations on MXene in the field of electrochemical NRR are rapidly proceeding, therefore, it is necessary to make a comprehensive summary of applications for MXene-based materials in this field. Herein, we firstly discussed the recent progress concerning the electrochemical NRR using MXene and MXene hybrids as catalysts, and then discussed the fabrication and surface modification of MXene, which might pave a new way to design MXene-based catalysts for conversion of N_2 into NH_3. Finally, the future research and challenge on MXenes for electrochemical NRR applications were discussed.

* Corresponding author.
E-mail address: yhxu@qdu.edu.cn (Y. Xu).
[1] These authors contributed equally to this work.

https://doi.org/10.1016/j.cclet.2020.01.035
1001-8417/

2. MXene-based catalysts for electrochemical NRR

Due to the intrinsically strong chemical bonds of N_2, a mass of energy are required to surmount the kinetic limitation of NH_3 synthesis. Therein, well-designed catalysts will provide a lower-energy pathway for the reaction to occur, allowing the reaction to proceed under relatively mild conditions. Recently, many works have been devoted to exploring MXene catalysts for the electrochemical NRR. To sum up, two types of electrocatalysts based on their chemical composition have been reported, including pure MXene electrocatalysts and MXene-based hybrid ones. In the subsequent sections, we will detail recently reported MXene-based electrocatalysts for NRR.

2.1. Pure MXene catalysts for electrochemical NRR

Recently, density functional theory (DFT) calculations on M_3C_2 transition metal carbides MXene demonstrated that they could be promising catalysts for N_2 capture and reduction [27]. Among the M_3C_2 carbides (M = Ti, Zr, Hf, V, Nb, Ta, Cr and Mo), V_3C_2 and Nb_3C_2 exhibit the most outstanding features for NRR with the maximum over-potentials of 0.64 eV and 0.90 eV, respectively (*vs.* standard hydrogen electrodes) (Fig. 1A). Compared with Nb_3C_2 (0.85 eV), V_3C_2 requires a lower activation energy barrier (0.64 eV) in the first step of N_2 hydrogenation (from N_2 to N-NH*), and the reaction profile is smooth and has a lower energy barrier for next hydrogenation process. Moreover, Gao *et al.* employed the DFT to predict the feasibility of Mo_2TiC_2 electrocatalyst for NH_3 synthesis [28]. The pathway becomes thermodynamically possible at the potential of 0.26 V. In addition, free energy for the hydrogen evolution reaction (HER) [29] on Mo_2TiC_2 indicates that HER has a much higher over-potential than NRR, meaning that N_2 will more easily occupy the Mo active sites. In other words, HER can be well suppressed. This indicates that the catalyst can get a higher Faradic efficiency (FE).

Wang and co-workers conducted an experimental study of Ti_3C_2 MXene nanosheets as catalysts for electrochemical NRR [30]. They used a mixture of HCl and LiF as an etchant to synthesize Ti_3C_2 MXene solution, and then they applied the ultrasonic method to obtained MXene flakes with a different scale. Scanning electron microscopy (SEM) image indicates that the exfoliated MXene flakes are very thin (Fig. 1B). DFT calculations were applied to explore the active sites on MXene for N_2 adsorption. As shown in Fig. 1C, the middle Ti atoms exhibit the highest N_2 adsorption (–1.34 eV) compared to other sites (*e.g.*, C, O and lateral Ti). The Ti_3C_2 nanosheets supported by stainless steel mesh (SSM) could achieve the FE of 4.62% and NH_3 yield rate of 4.72 μg h^{-1} cm^{-2} at –0.1 V *vs.* reversible hydrogen electrode (RHE). Through tailoring Ti_3C_2 MXene nanosheets to a smaller size and vertically arranging on the FeOOH nanosheet, the MXene/FeOOH showed poor HER activity while achieved a higher FE of 5.78% for NRR (Fig. 1D). Sun and co-workers etched the $Ti_3C_2T_x$ (T = F, OH) from the MAX (Ti_3AlC_2) phase using the mixture of HCl and LiF, and then reached the 2D $Ti_3C_2T_x$ nanosheets by intercalation with dimethylsulfoxide (DMSO) [31]. As shown in Fig. 2A, the obtained 2D $Ti_3C_2T_x$ nanosheets have a loosely layered structure. The TEM image (Fig. 2B), clearly indicated the flake-structure of the $Ti_3C_2T_x$ nanosheets, which showed excellent catalytic activity for NRR, achieving an NH_3 yield of 20.4 μg h^{-1} $mg_{cat.}^{-1}$ with a FE of 9.3% in acids buffer (Fig. 2C). Research showed that the F terminals limited

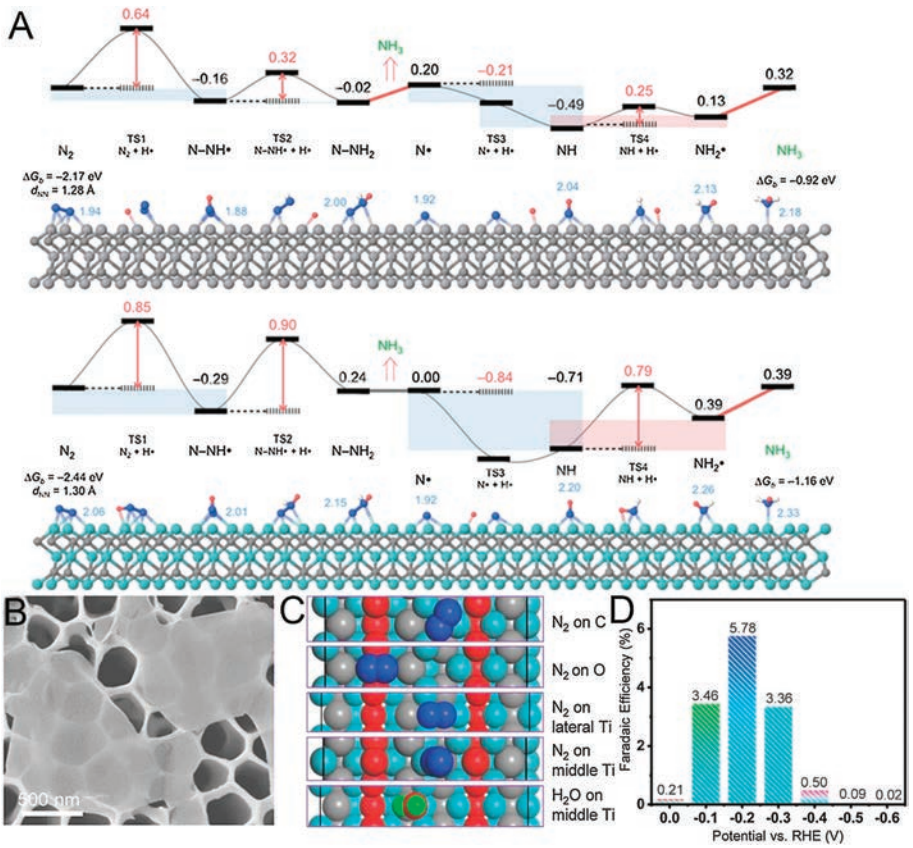

Fig. 1. (A) DFT + D3 calculation of N_2 conversion into NH_3 catalysed by V_3C_2 (top) and Nb_3C_2 (bottom) MXenes. Adapted with permission [27]. Copyright 2016, Royal Society of Chemistry. (B) SEM image of Ti_3C_2 nanosheets. (C) Snapshots of N_2 on various atomic sites of MXene. (D) FEs of Ti_3C_2 on FeOOH nanosheet. Adapted with permission [30]. Copyright 2018, Elsevier Ltd.

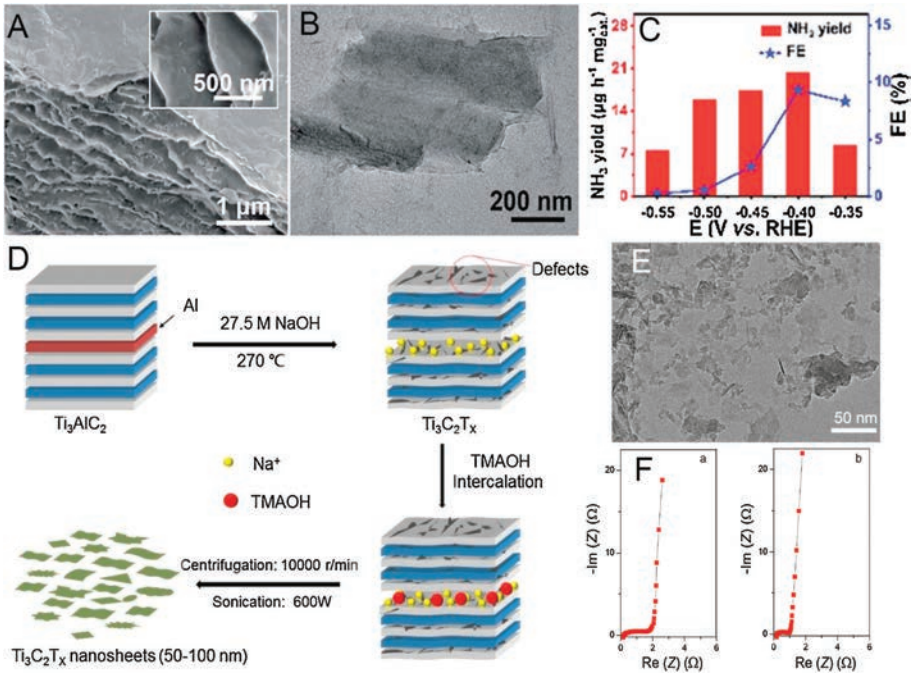

Fig. 2. (A) SEM and (B) TEM images of $Ti_3C_2T_x$ nanosheets. (C) NH_3 yields and FEs of $Ti_3C_2T_x$ nanosheets at a different potential. Adapted with permission [31]. Copyright 2018, Royal Society of Chemistry. (D) Scheme for the generation of NaOH-$Ti_3C_2T_x$ nanosheets. (E) TEM image of NaOH-$Ti_3C_2T_x$ nanosheets delaminated with TMAOH. (F) EIS data of (a) HF-$Ti_3C_2T_x$ and (b) NaOH-$Ti_3C_2T_x$. Adapted with permission [32]. Copyright 2019, Royal Society of Chemistry.

the applications of MXene in electrocatalysis because F is inactive, destroying the conductivity [21]. Wang and co-workers have demonstrated that Ti atoms on the edges were much favourable for the NRR. However, the MXene nanosheets prepared in previous works are too large to expose more Ti atoms. Zhang and co-workers applied an alkali-assisted route to obtain fluorine-free $Ti_3C_2T_x$ (T = O, OH) (NaOH-$Ti_3C_2T_x$) nanosheets with small size (50–100 nm) in their recent work [32]. Fig. 2D is the synthetic route of NaOH-$Ti_3C_2T_x$ nanosheets. TEM image of NaOH-$Ti_3C_2T_x$ nanosheets delaminate with TMAOH indicates that the lateral size of the nanosheets is 50–100 nm (Fig. 2E) Electrochemical impedance spectroscopy (EIS) measurement (Fig. 2F) proves that NaOH-$Ti_3C_2T_x$ nanosheets have better conductivity than $Ti_3C_2T_x$ nanosheets treated with HF (HF-$Ti_3C_2T_x$). The NH_3 yield of the NaOH-$Ti_3C_2T_x$ can reach a value of 36.9 μg h^{-1} $mg_{cat.}^{-1}$, ~1.59 times higher than the maximum value of HF-$Ti_3C_2T_x$ (23.2 μg h^{-1} $mg_{cat.}^{-1}$).

2.2. MXene hybrids catalysts for electrochemical NRR

2.2.1. Noble metal-MXene catalysts for electrochemical NRR

The above researches show that MXenes are promising NRR electrocatalyst. However, the pure one itself is still challenging to achieve the requirement of high catalytic efficiency. Subsequently, MXene hybrids can be designed for converting N_2 to NH_3. By avoiding the aggregation, the layered structure of MXene could enhance the chemical properties of the nanosized particles such as accelerating the electron transfer. The surface of MXene materials after Al-removing has a large number of functional groups (such as −OH, –F). Although the electrical conductivity and mechanical strength of MXenes are somewhat affected by these functional groups, these functional groups provide direction exchange sites and play a role of efficient reductant to some oxides [33]. The nanoscale metal particles formed on MXene surface create a great chance to improve its conductivity, increasing the performance in the applications of electrocatalysis. Alternatively, noble metal nanostructures and nanocomposites have shown remarkable electrochemical NRR activity [34–36].

In nature, the web woven by spider provides an obvious platform for the interaction between predators and prey, inspired by this, Li and co-workers designed an ideal system for efficient electrochemical NRR—a "web" (Ti_3C_2 nanosheets) for effective capture of N_2 and "predators" (Au nanoparticles) for N_2 conversion [37]. They used the mixture of LiF and HCl as an etchant to prepare Ti_3C_2 nanosheets, −OH on the surfaces of Ti_3C_2 could provide anchoring sites for Au nanoparticles. Then the nano-sized Au particles could be loaded onto the surface of Ti_3C_2 nanosheets (Au/Ti_3C_2) by ultrasound reduction approach.

TEM image (Fig. 3A) evidences that Au nanoparticles less than about 10 nm in diameter are distributed on the surface of Ti_3C_2 uniformly. Moreover, Li and co-workers found that certain Au with high chemical valence was preserved in the ultrasonic reduction process. Temperature programmed desorption of N_2 (N_2-TPD) dates show that the peak attributed to chemisorbed N_2 (at about 280 °C) of Au/Ti_3C_2 significantly increased relative to the Ti_3C_2. It indicates that Au with high valence promotes the chemical adsorption of N_2. Furthermore, it can be seen from the optimized geometry shown in the inset of Fig. 3B, the length of the N≡N bond extends from 1.154 Å to 1.365 Å after chemical adsorption of N_2 on the surface, indicating that Au promotes the dissociation of N≡N bond. The DFT calculation (Fig. 3C) shows that the high energy adsorbed by N_2 at the interface between the Au and Ti_3C_2 weakens the N≡N, and reduces the activation energy barrier. In the condition of 0.94% Au loading, Au/Ti_3C_2 shows an excellent average NH_3 yield of 30.06 μg h^{-1} $mg_{cat.}^{-1}$ with a high FE of 18.34%.

2.2.2. Transition metal oxide-MXene catalysts for electrochemical NRR

The wide applications of precious metal-based MXene hybrid materials for electrocatalysis are impeded to some extent by their high price. Non-noble metal-based materials, particularly transition metal (TM) oxide materials, have been widely applied as NRR electrocatalysts due to their earth-abundant reserves, and low

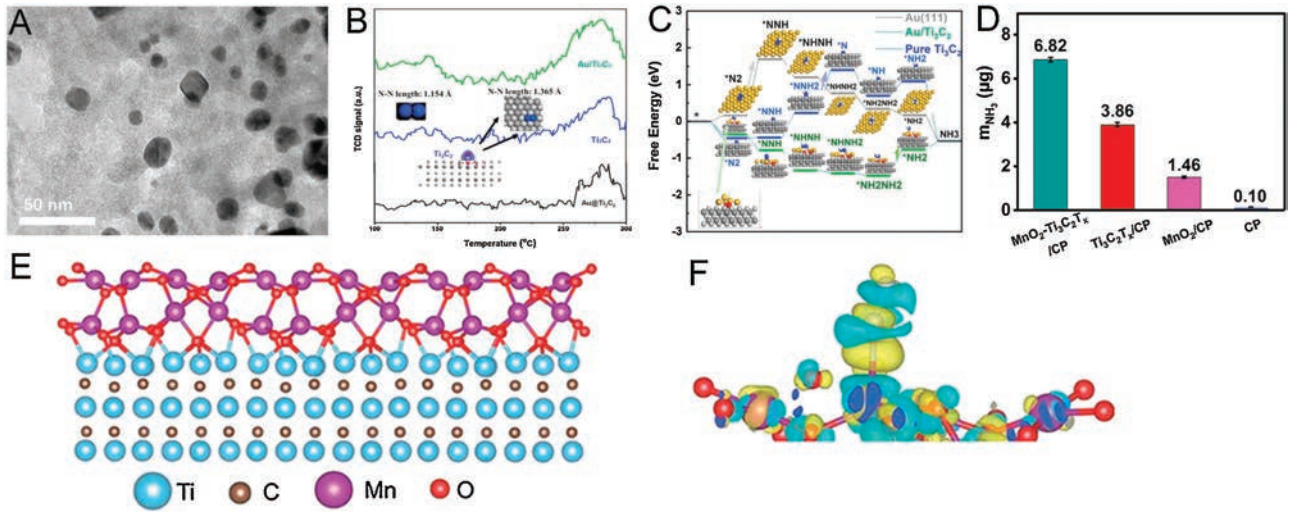

Fig. 3. (A) TEM image of Au/Ti_3C_2. (B) N_2-TPD dates of Ti_3C_2 (blue), Au@Ti_3C_2 (black) and Au/Ti_3C_2 (green). Inset: The adsorption geometry of N_2 on Ti_3C_2 and the change of N—N bond length after adsorption on Ti_3C_2. (Ti: light grey, C: dark grey, and N: blue). The blue and red isosurface denote the electron loss and accumulation, respectively. (C) Free energy profile for N_2 conversion into NH_3 pathways on Au (111), Ti_3C_2, and Au/Ti_3C_2 samples. Adapted with permission [37]. Copyright 2019, American Chemical Society. (D) Amount of NH_3 with different electrodes after 2 h electrolysis. (E) Optimized structure of the MnO_2-$Ti_3C_2T_x$ heterostructure and (F) deformation charge density plot of the N_2-adsorbed configuration on MnO_2-$Ti_3C_2T_x$ heterostructure surface. Adapted with permission [39]. Copyright 2019, Royal Society of Chemistry.

toxicity as well as availability of d-orbital electrons for π-back donation, which can activate N_2. However, their low conductivity is detrimental to electrochemical properties, which is expected to be enhanced by the supporting platforms of MXene [38]. Accordingly, MnO_2-decorated $Ti_3C_2T_x$ (MnO_2-$Ti_3C_2T_x$) could function as an electrocatalyst for efficient N_2-to-NH_3 conversion at ambient conditions [39]. Such MnO_2-$Ti_3C_2T_x$ catalysts were obtained by direct chemical synthesis. $Ti_3C_2T_x$ improved the electrical conductivity of MnO_2, meanwhile prevented the aggregation during electrochemical processes. As shown in Fig. 3E, adsorption between N_2 and the MnO_2-$Ti_3C_2T_x$ heterostructure suggests that the unsaturated surface of Mn atoms could serve as active sites to adsorb and activate the N_2 molecules. This electrocatalyst achieved a high NH_3 yield rate (34.12 μg h^{-1} $mg_{cat.}^{-1}$) and FE (11.39%), respectively. Also, MnO_2 and $Ti_3C_2T_x$ have NRR activity as well (Fig. 3D). It is worth noting that MnO_2-$Ti_3C_2T_x$/CP (6.82 μg) exhibits greatly enhanced electrocatalytic NRR activity, ~4.7 times higher than MnO_2/CP (1.46 μg) and ~1.8 times higher than $Ti_3C_2T_x$/CP (3.86 μg), meaning that MnO_2 and $Ti_3C_2T_x$ promote electrocatalysis synergistically.

To further improve the FE of electrochemical N_2-to-NH_3 conversion, we used the marginal titanium atoms with thermodynamically metastable on the surface of $Ti_3C_2T_x$ MXene as nucleating site to successfully construct a heterojunction structure of TiO_2 nanoparticles distributed on the $Ti_3C_2T_x$ surface (TiO_2/$Ti_3C_2T_x$). Meanwhile, a mass of oxygen vacancies were introduced into the material to promote the performance of the NRR electrocatalysis. The TiO_2/$Ti_3C_2T_x$ was synthesized *via* a one-step ethanol-thermal strategy. DFT calculation showed N_2 can adsorb on the surfaces of different catalysts in the form of end-on mode, while Ti-edge atoms and oxygen vacancies could act as active sites to activate and polarize N_2 molecules. The free energy scheme indicated the lowest energy barrier of TiO_2/$Ti_3C_2T_x$ could compare to other samples. Accordingly, this electrocatalyst exhibited an NH_3 yield of 32.17 μg h^{-1} $mg_{cat.}^{-1}$ at –0.55 V *vs.* RHE with a FE of 16.07% at –0.45 V *vs.* RHE [40].

2.2.3. MXene-based single atom catalysts for electrochemical NRR

Recently, single atom catalysts (SACs) showed superb performance in NRR electrocatalysis systems [41]. The highly unsaturated metal atomically dispersed on a matrix exhibits excellent activity, and the strong interaction between the single atom and the matrix can efficiently anchor the individual atoms thus preventing their aggregation. Catalytic properties can be improved by coupling the active metal with suitable support. Chen and co-workers carried out DFT computations to investigate the NRR performance of the defective $Mo_2TiC_2O_2$ MXene nanosheets embedded with a series of TM atoms (including 3d, 4d and 5d except for Tc, Hg and lanthanide) ($Mo_2TiC_2O_2$-TM_{SA}) [42]. The barrier of possible potential-determination step—the highest energy barrier (ΔG_{max}) determines the thermodynamic possibility of the electrocatalytic process. As shown in Fig. 4A, the ΔG_{max} of candidates containing Zr, Mo, Hf, Ta, W, Re and Os are all quite low, indicating all of them exhibited excellent NRR performance. Among them, Zr-containing nanosheet ($Mo_2TiC_2O_2$-Zr_{SA}) has the lowest ΔG_{max} of 0.15 eV. From Fig. 4B, we can see these elements' limiting potentials for HER (U_L(HER)) and NRR (U_L(NRR)) potential, when U_L(NRR) < U_L(HER), the electrocatalysts are selective for NRR. Similarly, Zr has the lowest limiting potential.

3. The fabrication of MXenes

MXenes are widely applied in many fields, but the applications on electrochemical NRR are fewer than expected. This should be related to their complex preparation process. The removal of the interlayered A atoms of the MAX will lead to the formation of dangling bonds on the surface M atoms. Multifarious etching processes will result in different terminal group bonding to the M atoms. Therefore, the surface characteristics of MXene are closely related to the preparation method. Moreover, the etching conditions varied from the strength of the "A"-containing bonds. Suitable etching conditions are critical to achieving high yields and purity. Since the first experimental realization of $Ti_3C_2T_x$ in 2011 [21], many efforts have been devoted to seeking novel strategies to prepare a wide variety of MXene. Gogotsi and co-workers proposed that the $Ti_3C_2T_x$ can be easily separated from the MAX (Ti_3AlC_2) phase by etching the Al atoms selectively in hydrofluoric acid (HF) at room temperature [21]. Until now, on the methods of synthesizing MXene materials, as the most widely used and universal method, the HF etching method still play the important

A

	$\Delta E_{N2\text{-adsorption}}$ [eV]	PDS	ΔG_{max} [eV]	$\Delta G_{NH3\text{-desorption}}$ [eV]
Zr	−0.57	$^*N_2 \rightarrow {}^*NNH$	0.15	0.97
Mo	−0.58	$^*NH_2 \rightarrow {}^*NH_3$	0.51	0.58
Hf	−0.52	$^*NH \rightarrow {}^*NH_2$	0.25	0.98
Ta	−0.31	$^*NH \rightarrow {}^*NH_2$	0.21	0.77
W	−0.43	$^*NH \rightarrow {}^*NH_2$	0.46	0.81
Re	−0.51	$^*NH \rightarrow {}^*NH_2$	0.47	0.81
Os	−0.42	$^*NH \rightarrow {}^*NH_2$	0.32	0.72

B

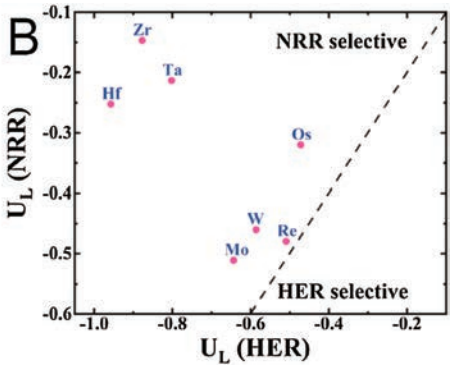

Fig. 4. (A) Detailed information of candidates. (B) Calculated limiting potentials for HER (U_L(HER)) and NRR (U_L(NRR)) on the surfaces of seven candidates. The dashed line represents U_L(HER) = U_L(NRR). When U_L(NRR) < U_L(HER), the electrocatalysts are selective for NRR. Adapted with permission [42]. Copyright 2019, Wiley-VCH.

role. However, HF is highly toxic and corrosive. There is thus an urgent need to explore effective, gentler, and harmless methods to synthesize MXene.

3.1. Modified acid etching method

To avoid the application of HF directly for extracting A atoms from MAX, firstly, the researchers used a mixture of HCl and fluoride salt (LiF, NaF, KF, CaF_2 and FeF_3) as an etchant in place of HF, called "*in situ* HF method" [43]. During the etching, the *in situ* formed HF selectively remove the A atoms from MAX. Besides, due to the intercalation of metal ions and water molecule into the interlayered space, the interlayered interaction of the obtained MXene layers became weaker. The nature of the mixture of HCl and fluoride salt compared with HF is much milder, so the MXene flakes did not have surface defects. Furthermore, instead of the HF etchant, ammonium bifluoride (NH_4HF_2) was also demonstrated as a new kind of etchant [44]. The intercalation of NH_3 and NH_4^+ species resulted in a 25% larger c-lattice parameter of the obtained MXene film than HF etching.

3.2. Molten fluoride salt etching method

Recently, most attention was still paid on the preparation of carbides and carbonitrides MXene, while nitrides MXene ($Ti_{n+1}N_nT_x$) were rarely studied. This should because the Al-N bond in $Ti_{n+1}AlN_n$ is stronger than Al-C bond in $Ti_{n+1}AlC_n$, accordingly, it is more difficult to etch Al in $Ti_{n+1}AlN_n$ [45]. More importantly, the nitrides have low cohesive energy, and the nitrogen-containing MXenes are less stable than the corresponding carbon-containing analogs. Therefore, $Ti_{n+1}N_nT_x$ would dissolve in the HF solution. To meet these challenges, Gogotsi and co-workers prepared nitrides MXene ($Ti_4N_3T_x$) by heating the mixture of Ti_4AlN_3 and ternary eutectic molten fluoride salt (LiF, NaF and KF) at 550 °C under Ar protection, as shown in Fig. 5A [46]. However, compared to other HF-etched titanium carbide MXenes, the delaminated $Ti_4N_3T_x$ showed inferior crystallinity [47]. This indicates that the molten fluoride salt etching method still has some problems in the preparation of nitride-based MXenes.

3.3. Alkaline etching method

The modified acid etching method avoids using HF directly, but there is still HF release in the solution. Inspired by the Bayer process widely used in the refining of bauxite, Zhang and co-workers proposed an alkali-assisted hydrothermal method using NaOH solution as an etchant to prepare a typical $Ti_3C_2T_x$ (T= −OH, −O) (Fig. 5B) [48]. They used high temperature (270 °C) condition to

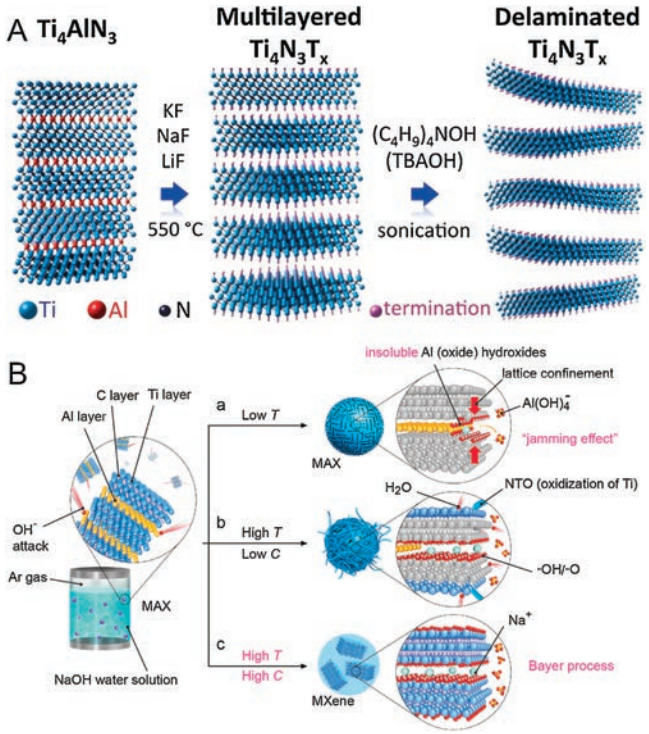

Fig. 5. (A) Schematic diagram of the preparation process of $Ti_4N_3T_x$ from Ti_4AlN_3 by molten salt treatment. Adapted with permission [46]. Copyright 2016, Royal Society of Chemistry. (B) Schematic of the reaction of the alkali-assisted hydrothermal method using NaOH solution. (a) Al (oxide) hydroxides prevent the Al extraction process at low temperatures. (b) Some Al (oxide) hydroxides dissolve in NaOH (low NaOH concentrations at high temperatures). In addition, higher water content causes the MXene to oxidize and yields NTOs. (c) Based on the Bayer process, high temperatures and high NaOH concentrations will dissolve Al (oxide) hydroxides in NaOH effectively. Adapted with permission [48]. Copyright 2018, Wiley-VCH.

promote the conversion of $Al(OH)_3$ and AlO(OH) to dissolvable Al $(OH)_4^-$, and the applied of highly alkaline concentrate (27.5 mol/L) with low water containment to prevent oxidation of Ti species. This Bayer process-based method is free of fluorine and could reach multilayer $Ti_3C_2T_x$ with a purity of ~92 wt%. This process avoids the release of HF, but it is necessary to heat concentrated NaOH solution under hydrothermal conditions of high temperature and pressure, this is also dangerous. To reduce the danger more effectively, Geng and co-workers proposed a milder method of organic-base-driven intercalation and delamination of Ti_3AlC_2, which used tetramethylammonium hydroxide (TMAOH) as an etchant (Fig. 6A) [49].

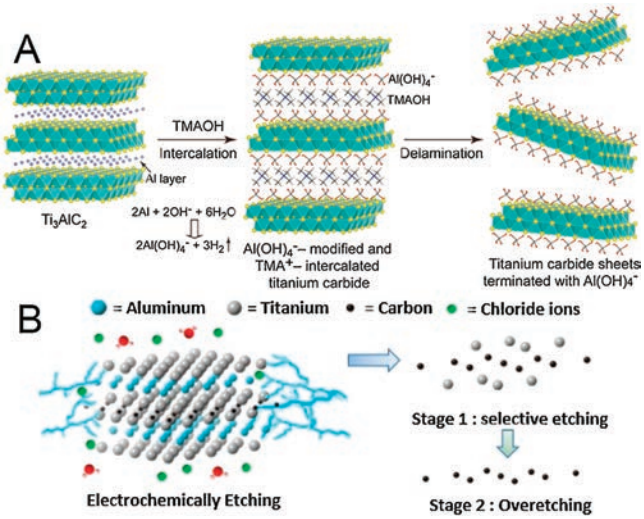

Fig. 6. (A) Schematic diagram of the insertion and delamination process. The organic base (TMAOH) reacts with the Al atomic layer in the gallery to promote key processes, including disrupt of the Ti-Al bonds by the way of Al hydrolysis, and the insertion of bulky TMA^+ into the gallery, in a single step. The disruption of Ti-Al metallic bonds and bulky-ion insertion contributes the succeeding disassembly of the precursor layered crystals into their elementary layers.Adapted with permission [49]. Copyright 2016, Wiley-VCH. (B) The electrochemical etching mechanism of Ti_2AlC with diluted HCl. Adapted with permission [52]. Copyright 2019, American Chemical Society.

Commercially, TMAOH is widely applied to etching Al. The $Al(OH)_4^-$ formed in the process of the Ti_3AlC_2 delamination can easily form a bond with the surface Ti atom, while the TMA^+ cation inserted the interlamellar space, thereby promoting delamination.

3.4. Electrochemical etching method

The electrochemical etching route has been proven to be an effective etching strategy for selectively extracting nanolayer materials from MAX precursors. However, there are still some unsatisfactory factors in the electrochemical etching method, such as a long etching period, less favourable for production scale, and toxicity of the intercalants [50,51]. Recently, Hao and co-workers developed a general strategy based on a thermally assisted electrochemical etching process to synthesize MXene (Ti_2CT_x, Cr_2CT_x, and V_2CT_x) [52]. The electrochemical etching route with diluted HCl is applied to prepare Ti_2CT_x. As shown in Fig. 6B, the etching process was divided into two phases: the voltage applied in stage 1 firstly etched Al atoms to form the layered carbide (Ti-Al bond is weaker than the Ti-C bond); in stage 2, both Al and Ti atoms were etched until only a single layer of carbon atoms remained. In addition, etching of Ti_2AlC can be accelerated by gentle heating. Moreover, the corresponding MXene can be prepared by applying different etching voltages (at 0.3 V *vs.* RHE for Ti_2AlC and 0.4–0.7 V for V_2AlC and 0.6–1.0 V for Cr_2AlC).

4. Surface modification of MXene

Surface modification of MXene can alter the surface chemistry of MXene by adjusting its interlayer distance, ion diffusion, and hydrophilicity/hydrophobicity [53]. Active sites that facilitate nitrogen adsorption and activation can also be introduced during the modification of MXene, such as Au/Ti_3C_2, $MnO_2/Ti_3C_2T_x$, and $TiO_2/Ti_3C_2T_x$ [37,39,40]. Among them, Au and MnO_2 acted as the active sites for adsorption and activation of N_2 in Au/Ti_3C_2 and MnO_2-$Ti_3C_2T_x$ catalysts, respectively, while the oxygen vacancies in $TiO_2/Ti_3C_2T_x$ were considered to be their active sites. In addition, these active sites and MXene could synergistically promote the performance of NRR. Therefore, classifications for MXene-based nanocomposites are important to facilitate the study of NRR catalysts.

4.1. Inorganic and polymer modification of MXene

Several recent reports have comprehensively reviewed the current surface modification of MXene [54,55]. In brief, a series of MXene-based inorganic nanostructure have been investigated, which include noble metal (Au [34], Ag [56], Pt [57], Ru [58], *etc.*), transition metal oxide-MXene materials (TiO_2 [40]), MnO_2 [39], Fe_2O_3 [59], Nb_2O_5 [60], *etc.*), metal hydroxide [61], and chalcogenides [62]. Moreover, the incorporation of polymers into conductive MXene substrates provides a unique set of physico-chemical properties such as variable band gaps, mechanical stiffness, controlled charge transport. MXene-polymer composites are fascinating materials for electrochemical applications [63,64]. In addition to inorganic nanostructures and polymers, other materials such as carbon nanotubes, graphene, biomaterials, and MOF have also been hybridized with MXene for applying in the field of electrochemistry [55].

4.2. Heteroatom doping on MXene

To further promote the electrochemical performance of MXene, the introduction of heteroatom doping such as non-metallic atoms with low electronegativity into MXene can be a fashionable strategy. Heteroatom doping on MXene can effectively increase the intrinsic activity and improve the distribution of atomic charge density and/or spin density, contributing to the enhancement of the electrochemical properties of the doped materials [53,55,65]. An and co-workers used cyanamide as the interlayer intercalation agent and nitrogen source, applying the step-by-step strategy to synthesize a highly N-doped Ti_2CT_x (Fig. 7A) [65]. Cyanamid forms p-C_3N_4 on the surface of Ti_2CT_x nanosheets by condensation reaction at 500–700 °C, which promotes delamination of Ti_2CT_x, followed by heat treatment of p-C_3N_4 and Ti_2CT_x complexes at 900 °C, nitrogen species can be doped into the inner carbon layer and/or defect sites of the Ti_2CT_x nanosheets (N doping amount 15.48%). The synergistic effect of 2D structure and heteroatoms doping capacitor electrode with high capacitance makes such highly N-doped Ti_2CT_x an excellent electrochemical. Wang and co-workers employed one-step thermal annealing to synthesize N-doped $Ti_3C_2T_x$ (N-$Ti_3C_2T_x$) [67]. They used the electrostatic self-assembly between $Ti_3C_2T_x$ with negatively charge and melamine with positively charge as precursors. This nitrogen doping strategy gives N-$Ti_3C_2T_x$ a porous structure, a high surface area and strong physical and chemical adsorption capacity.

Recently, phosphorous doped V_2CT_x MXene was obtained by a simple heat treatment approach with triphenylphosphine as a phosphorous source (Fig. 7B) [53]. This approach can control chemical composition according to the phosphorylation temperature to optimize the chemical structure. DFT calculations proved that P—C bonding reveals the lowest surface formation energy and Gibbs free energy compared to others such as P-oxide and P–V (phosphide). In addition, Xu and co-workers not only introduced P but also O into the Mo_2CT_x MXenes (P-Mo_2CT_x) through a simple phosphating strategy with red phosphorus as the P source [68]. The enhanced electrochemical performance of P-Mo_2CT_x can be attributed to the following factors: first, the expanded interlayer distance and the introduced P and O elements could increase the active sites; second, the introduction of P can improve the conductivity of P-Mo_2CT_x. Besides, the N and S doping strategy was also effective to increase interlayer spacing and enhance the conductivity of MXene (Fig. 7C) [66].

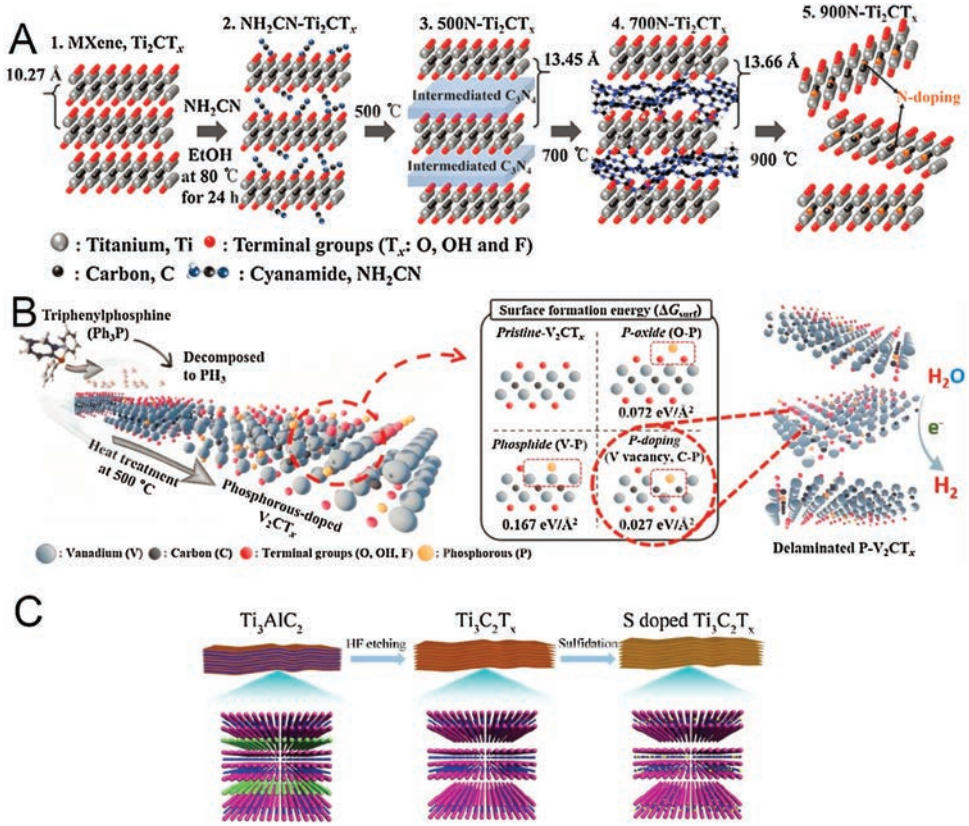

Fig. 7. (A) Schematic illustration of the synthesis of 900N-Ti_2CT_x. Adapted with permission [65]. Copyright 2018, Wiley-VCH. (B) Synthesis procedures of the P-doped V_2CT_x nanosheets by heat treatment with triphenyl phosphineand and their possible chemical compositions which can be determined by calculated surface formation energy. Adapted with permission [53]. Copyright 2018, Wiley-VCH. (C) Synthesis procedures of the preparation of S-doped $T_3C_2T_x$. Adapted with permission [66]. Copyright 2017, Royal Society of Chemistry.

5. Summary and outlook

MXene-based materials have many attractive properties such as high surface area, tunable electronic structure and high electronic conductivity all make a promising material for electrocatalysis applications. In order to further explore their application, it is necessary to better understand the MXene materials. In this concept article, we have summarized the applications of MXene-based nanomaterials as emerging catalysts for electrochemical NRR, including pure MXene and MXene hybrids. Efforts have shown that MXene-based nanomaterials have achieved great performances in this field, indicating that these are very promising materials as electrocatalysts for NRR. Moreover, we have outlined the fabrication of MXenes and the surface modification of MXenes.

It can be predicted that MXene-based hybrid will yield unusually brilliant results in electrocatalytic nitrogen fixation shortly. However, researches on MXene-based catalysts are mainly focused on Ti-based MXene at a nascent stage. Works of other metal-based MXene (including V, Nb, Cr, Mo, *etc.*) in electrocatalysis of N_2-to-NH_3 conversion have rarely been reported. When it is used as electrode materials, the two-dimensional MXene materials easily aggregate and stack. Although the reaction activity and transmission rate of electrolyte ions can be enhanced *via* being inserted with inorganic metal ions, organic molecules, polymer molecules and CNTs between layers, ion transfer rate will exponentially decrease with increasing the thickness of the electrode material. As for the preparation of MXenes, most of the preparation methods of MXenes at present are top-down ones using harmful reagent (*e.g.*, HF) and complicated conditions, so greener and more efficient preparation methods such as electrochemical ones should be promoted. Although considerable progress has been made in NRR by MXene, it is still far from the industrialization. But it can be promoted from the following aspects. (1) We need to develop a green, non-toxic and efficient method for large-scale preparation of MXenes. (2) Several MXenes with high catalytic activity and good stability should be selected for nitrogen reduction, and the reagents for modifying the MXene should be cost-effective. (3) Finally, more diverse MXenes categories should be investigated through the combination of theoretical prediction and experimental research. Moreover, identifying the catalytic nature and elucidating the catalytic mechanism in MXene-based catalysts remain a challenge. Therefore, considering the great potential of MXene-based catalysts in electronic hydrogenation of N_2 for NH_3, various MXenes should be investigated through the combination of theoretical prediction and experimental research.

Declaration of competing interest

The authors declare that they have no known competing financial interests or personal relationships that could have appeared to influence the work reported in this paper.

Acknowledgments

This work was supported by the National Natural Science Foundation of China (Nos. 21874079 and 20575071), Natural Science Foundation for Outstanding Young Scientists of Shandong Province (No. ZR2018JL011), Key R&D Project of Shandong Province (No. GG201809230180), Qingdao Science & Technology Planning

Project (No. 17-6-3-15-gx), Science & Technology Fund Planning Project of Shandong Colleges and Universities (No. J16LA13&J18KA112) and Taishan Scholars Program of Shandong Province (No. tsqn201909088).

References

[1] S. Chu, A. Majumdar, Nature 488 (2012) 294–303.
[2] J. Liang, D. Chen, X. Yao, et al., Small 15 (2019) 1903398.
[3] V. Rosca, M. Duca, M.T. de Groot, M.T. Koper, Chem. Rev. 109 (2009) 2209–2244.
[4] R. Service, Science 345 (2014) 610.
[5] J.G. Chen, R.M. Crooks, L.C. Seefeldt, et al., Science 360 (2018) eaar6611.
[6] X. Guo, H. Du, F. Qu, J. Li, J. Mater. Chem. A 7 (2019) 3531–3543.
[7] B.H. Suryanto, H.L. Du, D. Wang, et al., Nat. Catal. 2 (2019) 290–296.
[8] V. Smil, Enriching the Earth: Fritz Haber, Carl Bosch, and the Transformation of World Food Production, MIT press, 2004.
[9] J. Yang, Y. Guo, W. Lu, R. Jiang, J. Wang, Adv. Mater. 30 (2018) 1802227.
[10] H.P. Jia, E.A. Quadrelli, Chem. Soc. Rev. 43 (2014) 547–564.
[11] G. Zhang, Q. Ji, K. Zhang, et al., Nano Energy 59 (2019) 10–16.
[12] V. Kyriakou, I. Garagounis, E. Vasileiou, A. Vourros, M. Stoukides, Catal. Today 286 (2017) 2–13.
[13] C. Guo, J. Ran, A. Vasileff, S.Z. Qiao, Energy Environ. Sci. 11 (2018) 45–56.
[14] K. Novoselov, A. Mishchenko, A. Carvalho, A.C. Neto, Science 353 (2016) aac9439.
[15] Q. Fu, X. Bao, Chem. Soc. Rev. 46 (2017) 1842–1874.
[16] L. Cong, H. Xie, J. Li, Adv. Energy Mater. 7 (2017) 1601906.
[17] M. Sun, H. Liu, J. Qu, J. Li, Adv. Energy Mater. 6 (2016) 1600087.
[18] B.H.R. Surrnto, D.B. Wang, L.M. Azofra, et al., ACS Energy Lett. 4 (2019) 430–435.
[19] J. Deng, C. Liu, Chem 4 (2018) 1773–1774.
[20] S.J. Luo, X.M. Li, B.H. Zhang, Z.L. Luo, M. Luo, ACS Appl. Mater. Interfaces 11 (2019) 26891–26897.
[21] M. Naguib, M. Kurtoglu, V. Presser, et al., Adv. Mater. 23 (2011) 4248–4253.
[22] P. Zhang, D.J. Wang, Q.Z. Zhu, et al., Nano-micor Lett. 11 (2019) 81.
[23] Y.T. Liu, P. Zhang, N. Sun, et al., Adv. Mater. 30 (2018) 1707334.
[24] Y. Zhong, X. Xia, F. Shi, et al., Adv. Sci. 3 (2016) 1500286.
[25] Z. Li, Y. Wu, Small 15 (2019) 1804736.
[26] Q. Zhao, Q.Z. Zhu, J.W. Miao, et al., Small 15 (2019) 1904293.
[27] L.M. Azofra, N. Li, D.R. MacFarlane, C. Sun, Energy Environ. Sci. 9 (2016) 2545–2549.
[28] Y. Gao, Y. Cao, H. Zhuo, et al., Catal. Today 339 (2018) 120–126.
[29] H. Du, R. Kong, X. Guo, F. Qu, J. Li, Nanoscale 10 (2018) 21617–21624.
[30] Y. Luo, G.F. Chen, L. Ding, et al., Joule 3 (2019) 279–289.
[31] J.X. Zhao, L. Zhang, X.Y. Xie, et al., J. Mater. Chem. A 6 (2018) 24031–24035.
[32] T. Li, X. Yan, L. Huang, et al., J. Mater. Chem. A 7 (2019) 14462–14465.
[33] Y. Ying, Y. Liu, X. Wang, et al., ACS Appl. Mater. Interfaces 7 (2015) 1795–1803.
[34] Y. Yang, S.Q. Wang, H. Wen, et al., Angew. Chem. Int. Ed. 131 (2019) 15506–15510.
[35] Z.H. Xue, S.N. Zhang, Y.X. Lin, et al., J. Am. Chem. Soc. 141 (2019) 14976–14980.
[36] H.K. Lee, C.S.L. Koh, Y.H. Lee, et al., Sci. Adv. 4 (2018) eaar3208.
[37] D. Liu, G. Zhang, Q. Ji, Y. Zhang, J. Li, ACS Appl. Mater. Interfaces 11 (2019) 25758–25769.
[38] N. Sun, Q.Z. Zhu, B. Anasori, et al., Adv. Funct. Mater. 29 (2019) 1906282.
[39] W. Kong, F. Gong, Q. Zhou, et al., J. Mater. Chem. A 7 (2019) 18823–18827.
[40] Y.F. Fang, Z.C. Liu, J.R. Han, et al., Adv. Energy Mater. 9 (2019) 1803406.
[41] X. Liu, Y. Jiao, Y. Zheng, M. Jaroniec, S.Z. Qiao, J. Am. Chem. Soc. 141 (2019) 9664–9672.
[42] L. Li, X.Y. Wang, H.R. Guo, et al., Small Methods 3 (2019) 1900337.
[43] X. Wang, C. Garnero, G. Rochard, et al., J. Mater. Chem. A 5 (2017) 22012–22023.
[44] A. Feng, Y. Yu, F. Jiang, et al., Ceram. Int. 43 (2017) 6322–6328.
[45] M. Naguib, V.N. Mochalin, M.W. Barsoum, Y. Gogotsi, Adv. Mater. 26 (2014) 992–1005.
[46] P. Urbankowski, B. Anasori, T. Makaryan, et al., Nanoscale 8 (2016) 11385–11391.
[47] M. Alhabeb, K. Maleski, B. Anasori, et al., Chem. Mater. 29 (2017) 7633–7644.
[48] T. Li, L. Yao, Q. Liu, et al., Angew. Chem. Int. Ed. 57 (2018) 6115–6119.
[49] J. Xuan, Z. Wang, Y. Chen, et al., Angew. Chem. Int. Ed. 55 (2016) 14569–14574.
[50] W. Sun, S.A. Shah, Y. Chen, et al., J. Mater. Chem. A 5 (2017) 21663–21668.
[51] S. Yang, P. Zhang, F. Wang, et al., Angew. Chem. Int. Ed. 57 (2018) 15491–15495.
[52] S.Y. Pang, Y.T. Wong, S. Yuan, et al., J. Am. Chem. Soc. 141 (2019) 9610–9616.
[53] Y. Yoon, A.P. Tiwari, M. Choi, et al., Adv. Funct. Mater. 29 (2019) 1903443.
[54] H. Yu, Y. Wang, Y. Jing, et al., Small 15 (2019) 1901503.
[55] H. Wang, Y. Wu, X. Yuan, et al., Adv. Mater. 30 (2018) 1704561.
[56] G. Zou, Z. Zhang, J. Guo, et al., ACS Appl. Mater. Interfaces 8 (2016) 22280–22286.
[57] X. Xie, S. Chen, W. Ding, Y. Nie, Z. Wei, Chem. Commun. 49 (2013) 10112–10114.
[58] X. Li, C. Zeng, G. Fan, Int. J. Hydrogen Energy 40 (2015) 9217–9224.
[59] H. Zhang, M. Li, J. Cao, et al., Ceram. Int. 44 (2018) 19958–19962.
[60] C.J. Zhang, S.J. Kim, M. Ghidiu, et al., Adv. Funct. Mater. 26 (2016) 4143–4151.
[61] Y. Wang, H. Dou, J. Wang, et al., J. Power Sources 327 (2016) 221–228.
[62] J. Ran, G. Gao, F.T. Li, et al., Nat. Commun. 8 (2017) 13907.
[63] M. Boota, M. Pasini, F. Galeotti, et al., Chem. Mater. 29 (2017) 2731–2738.
[64] M. Zhu, Y. Huang, Q. Deng, et al., Adv. Energy Mater. 6 (2016) 1600969.
[65] Y. Yoon, M. Lee, S.K. Kim, et al., Adv. Energy Mater. 8 (2018) 1703173.
[66] J. Li, D. Yan, S. Hou, et al., J. Mater. Chem. A 6 (2018) 1234–1243.
[67] W. Bao, L. Liu, C. Wang, et al., Adv. Energy Mater. 8 (2018) 1702485.
[68] G. Qu, Y. Zhou, T. Wu, et al., ACS Appl. Energy Mater. 1 (2018) 7206–7212.